

1 **Boron doped TiO₂ catalysts for photocatalytic ozonation of aqueous mixtures of**
2 **common pesticides: Diuron, o-phenylphenol, MCPA and terbuthylazine**

3
4 **D.H. Quiñones¹, A. Rey^{1*}, Pedro M. Álvarez¹, F.J. Beltrán¹, G. Li Puma²**

5 *¹Dpto. Ingeniería Química y Química Física, Universidad de Extremadura, Avda. Elvas*
6 *s/n 06006 Badajoz (Spain)*

7 *²Environmental Nanocatalysis and Photoreaction Engineering, Department of Chemical*
8 *Engineering, Loughborough University, LE11 3TU, Loughborough (United Kingdom)*

9
10 **Abstract**

11 TiO₂ and B-doped TiO₂ catalysts were synthesized using a sol-gel procedure. The
12 photocatalysts were characterized by ICP-EOS, N₂ adsorption-desorption, XRD, XPS,
13 and DR-UV-Vis spectroscopy. Four recalcitrant pesticides (diuron, o-phenylphenol, 2-
14 methyl-4-chlorophenoxyacetic acid (MCPA) and terbuthylazine) were subjected to
15 degradation by ozonation, photolytic ozonation, photocatalysis and photocatalytic
16 ozonation using the prepared catalysts under simulated solar irradiation in a laboratory
17 scale system. The B-doped TiO₂ catalysts, with 0.5-0.8 wt.% of interstitial boron, were
18 more active than bare TiO₂ for the removal and mineralization of the target compounds.
19 The combination of ozonation and photocatalysis led to faster mineralization rates than
20 the treatment methods considered individually and allowed the complete removal of the
21 pesticides below the regulatory standards. The B-doped catalyst was stable and
22 maintained 75% mineralization after three consecutive runs.

23
24 **Keywords**

25 Photocatalytic ozonation, boron doped TiO₂, boron leaching, pesticides, solar light.
26
27
28
29
30
31
32
33

1 1. Introduction

2 Water pollution and scarcity is a global concern. Agriculture is the industrial activity that
3 has the major impact on aquatic ecosystems, due to the large volumes of water
4 consumed (70% of the world accessible freshwater [1]) and the high content of organic
5 substances (pesticides and fertilizers) which are dispersed in aqueous environments by
6 runoff or leaching. Many pollutants found in water ecosystems are recalcitrant to some
7 degree to biological and physicochemical processes that are conventionally used in
8 wastewater treatment plants. In the last decades, Advanced Oxidation Processes
9 (AOPs) have being pointed out as effective alternatives to deal with this kind of
10 contaminants. These technologies can generate non-selective, highly reactive and
11 short-life oxidizing species, which in turn can completely degrade organic pollutants
12 through oxidation reactions [2].

13 Photocatalysis is one of the most successfully and extensively studied AOP. It involves
14 the excitation of a semiconductor through the absorption of photons having energy
15 greater than its band gap. This excitation promotes an electron from the valence to the
16 conduction band, which triggers a series of oxidation-reduction reactions involving the
17 excited electron and the generated hole at the valence band [2]. Recently, solar-driven
18 TiO₂ photocatalytic oxidation has attracted considerable attention in water treatment
19 applications. It offers the possibility of using solar energy to activate the semiconductor.
20 However, due to the TiO₂ wide band gap (3.2 eV) its photoactivity is limited to
21 ultraviolet irradiation ($\lambda < 380$ nm) and thus less than 5% of the solar spectrum can be
22 exploited [3]. In general, doping TiO₂ appears to be an effective way to overcome this
23 limitation, since the photoactivity of the doped semiconductor may be extended to the
24 visible-light region [4,5]. Boron doping constitute a way to accomplish it, since O atoms
25 in the TiO₂ lattice can be substituted by B atoms mixing the p orbital of B with O 2p
26 orbitals, narrowing the band gap and thus shifting the optical response into the visible
27 range [5]. On the other hand, boron can also be located in interstitial positions of the
28 TiO₂ lattice leading to the partial reduction of Ti(IV) to Ti(III), which could act as an
29 electron trap enhancing the photocatalytic activity of TiO₂ [5,6].

30 Another way to improve the performance of TiO₂ photocatalytic systems is its
31 simultaneous application with other AOPs, such as ozonation. The combined application
32 of ozone and TiO₂ photocatalysis, known as photocatalytic ozonation, leads to a
33 synergistic effect due to enhanced production of reactive oxygen species (ROS) such
34 as hydroxyl radicals in comparison with the application of either single ozonation or
35 single TiO₂ photocatalysis [7,8].

36 In this study, the degradation of four herbicides and pesticides: diuron (DIU), o-
37 phenylphenol (OPP), 2-methyl-4-chlorophenoxyacetic acid (MCPA) and terbuthylazine
38 (TBA), commonly found in water ecosystems, has been studied. Their molecular
39 structures can be found in **Table S1** of the supplementary material. The degradation
40 methods used were photocatalysis, ozonation, photolytic ozonation, and photocatalytic
41 ozonation. Different boron doped TiO₂ photocatalysts (B-TiO₂) were synthesized and
42 used in the photocatalytic treatments.

1 2. Experimental section

2 2.1. Catalysts preparation

3 The synthesis of TiO₂ and B-TiO₂ catalysts was carried out following a sol-gel
4 procedure previously reported [9]. Initially, a precursor solution was prepared by
5 diluting the required amount of boric acid (Fisher Scientific) in 10 mL anhydrous
6 ethanol (Panreac, 99.5%), then adding 4.26 mL tert-butyl titanate (Sigma Aldrich,
7 97%), adjusting the pH to 3-4 with glacial acetic acid (Merck) and stirring for 30 min.
8 After that, 20 mL ethanol were added to the precursor solution and the stirring was kept
9 for 2 more hours. Ammonia aqueous solution (Fisher Scientific, 35%) was then added
10 dropwise to reach pH 9. Afterward 10 mL ethanol was added and stirring was kept for
11 another 30 min. The suspension was centrifuged and washed with ethanol three times.
12 The resulting solid was dried at 60°C overnight, manually grinded and finally calcined
13 at 500°C for 30 min. Catalysts with 3, 6, 9 and 12 wt.% of B were prepared. The
14 nomenclature and some parameters of the catalysts are shown in **Table 1**. A fraction of
15 catalysts with 6 and 12 wt.% of B were washed with ultrapure water to analyze the
16 effect of B leaching.

17 2.2. Characterization of the catalysts

18 The characterization of the catalysts was carried out by inductively coupled plasma
19 optical spectroscopy, N₂ adsorption-desorption, X-ray diffraction (XRD), X-ray
20 photoelectron spectroscopy (XPS), and DR-UV-Vis spectroscopy.

21 Total B content of the catalysts was analyzed by inductively coupled plasma with an
22 ICP-OES Optima 3300DV (Perkin-Elmer) after acidic microwave digestion of the
23 samples.

24 BET surface area and pore structure of catalysts were determined from their nitrogen
25 adsorption-desorption isotherms obtained at -196°C using an Autosorb 1 apparatus
26 (Quantachrome). Prior to analysis the samples were outgassed at 250°C for 12 h under
27 high vacuum (<10⁻⁴ Pa).

28 The crystalline structure was analyzed by X-ray diffraction (XRD) using a Bruker D8
29 Advance XRD diffractometer with a CuK α radiation ($\lambda = 0.1541$ nm). The data were
30 collected from $2\theta = 20^\circ$ to 80° at a scan rate of 0.02 s⁻¹ and 1 s per point.

31 XPS spectra were obtained with a K α Thermo Scientific apparatus with an Al K α
32 ($h\nu=1486.68$ eV) X-ray source using a voltage of 12 kV under vacuum (2×10^{-7} mbar).
33 Binding energies were calibrated relative to the C1s peak at 284.6 eV.

34 Diffuse reflectance UV-Vis spectroscopy (DR-UV-Vis) measurements, useful for the
35 determination of the semiconductor band gap, were performed with an UV-Vis-NIR
36 Cary 5000 spectrophotometer (Varian-Agilent Technologies) equipped with an
37 integrating sphere device.

1 Transmitted photon flux through a catalyst suspension was analyzed by actinometrical
2 measurements following the method proposed by Loddo et al. in [10], using the solar
3 simulator described below with 250 mL of actinometrical solution and 250 mL of
4 catalyst suspension at 0.33 g L⁻¹. Incident radiation flux was determined with ultrapure
5 water replacing the catalyst suspension and was found to be 8.96x10⁻⁴ einstein min⁻¹.

6 **2.3. Photocatalytic activity measurements**

7 Photocatalytic experiments were carried out in a laboratory-scale system consisting of
8 a 250 mL pyrex made 3-neck round-bottom flask (8.8 cm outer diameter) provided with
9 a gas inlet, a gas outlet and a liquid sampling port. The reactor was placed in the
10 chamber of a commercial solar simulator (Suntest CPS, Atlas) equipped with a 1500 W
11 air-cooled Xe lamp with emission restricted to wavelengths over 300 nm (quartz and
12 glass cut-off filters). The emission spectrum of the solar simulator can be seen in
13 **Fig.S1** of the supplementary material. The irradiation intensity was kept at 550 W m⁻²
14 and the temperature of the system was maintained between 25 and 40°C throughout
15 the experiments. If required, a laboratory ozone generator (Anseros Ozomat Com AD-
16 02) was used to produce a gaseous ozone-oxygen stream that was fed to the reactor.

17 In a typical photocatalytic ozonation experiment, the reactor was first loaded with 250
18 mL of an aqueous solution containing 5 mg L⁻¹ initial concentration of each pesticide (in
19 a mixture). Then, the catalyst was added at a concentration of 0.33 g L⁻¹ and the
20 suspension was stirred in the darkness for 30 min (dark adsorption stage). Then, the
21 lamp was switched on and, simultaneously, a mixture of ozone-oxygen (5 mg L⁻¹ ozone
22 concentration) was fed to the reactor at a flow rate of 10 L h⁻¹. The irradiation time for
23 each experiment was 2 h. Samples were withdrawn from the reactor at intervals and
24 filtered through a 0.2 µm PET membrane to remove the photocatalyst particles.

25 Photolysis experiments (i.e. absence of catalyst and ozone), adsorption (i.e., absence
26 of radiation and ozone), ozonation alone (i.e., absence of radiation and catalyst), and
27 photolytic ozonation (i.e., absence of catalyst) were also carried out for comparative
28 purposes.

29 Pesticides concentrations were analyzed by HPLC (Hewlett Packard) provided with a
30 Kromasil C18 column (5 µm, 150 mm long, 4 mm diameter, Teknokroma). As mobile
31 phase a mixture of acetonitrile (solvent A) and 0.1% (v/v) phosphoric acid solution
32 (solvent B) was used at 1 mL·min⁻¹. Initially the mobile phase composition was varied from
33 40 to 25% solvent A in 12.5 min, then varied to 40% in 7.5 min and finally maintained at that
34 composition for more 10 min. The retention times for DIU, MCPA, TBA and OPP were 10,
35 15.2, 23.2 and 25.8 min, respectively. The detection system was set at 220 nm.

36 Total organic carbon content (TOC) was measured using a Shimadzu TOC-V_{SCH} analyzer.
37 Dissolved ozone was measured photometrically by following the indigo method at 600
38 nm [11]. Ozone in the gas phase was continuously monitored by means of an Anseros
39 Ozomat GM-6000Pro analyzer. Hydrogen peroxide concentration was determined
40 photometrically by the cobalt/bicarbonate method at 260 nm [12]. Boron leached from
41 the catalysts was determined photometrically after complexation with azomethine-H at

1 410 nm [13]. Photometric measurements were carried out in a UV-Visible
2 spectrophotometer (Evolution 201, Thermospectronic).

3 4 **3. Results and discussion**

5 **3.1. Catalysts characterization**

6 **Table 1** summarizes some characteristics of the B-doped TiO₂ catalysts. Firstly, it can
7 be noticed that the amounts of B incorporated to the catalysts are much lower than the
8 theoretical values. Similar results have been observed in previous studies where
9 around only 5-10% of the theoretical B was introduced in the final catalyst following sol-
10 gel synthesis techniques [14, 15].

11 The structure of the catalysts was analyzed by means of XRD and diffraction patterns
12 are shown in **Fig.1**. Anatase was identified as the only TiO₂ crystalline phase in all the
13 catalysts together with the appearance of the sassolite boron structure (H₃BO₃) with the
14 main diffraction peak at 2θ=28° for the catalysts with B content equal or greater than
15 the theoretical 6 wt.%. In addition, from the XRD patterns it can also be noticed that
16 anatase diffraction peaks intensity decreased with the increasing B content. The
17 crystallite size of anatase in the catalysts was calculated through Scherrer's equation.
18 The values, which are shown in **Table 1**, reveal that the crystal size decreases with the
19 increasing B content. This effect has been previously reported for similar catalysts and
20 it has been attributed to the restrained TiO₂ crystal growing due to the existence of
21 large amount of boron [16, 17, 18].

22 Textural parameters (BET surface area and total pore volume) were calculated from
23 the adsorption-desorption isotherms presented in **Fig.S2** of the supplementary
24 information and are summarized in **Table 1**. In general, the sol-gel synthesis procedure
25 together with the relatively short time of calcination led to catalysts with fairly high
26 surface areas. In addition, it can be observed that both, BET surface area and total
27 pore volume, increased with the increasing B content, effect that can be attributed to
28 the lower crystal size of the anatase phase in the B-TiO₂ catalysts [16].

29 Surface composition of the TiO₂ and B-TiO₂ catalysts was analyzed by XPS. **Fig.2A**
30 shows, as an example, the high-resolution XPS spectra of the B 1s spectral region
31 corresponding to 12B-TiO₂ catalyst. The binding energy for B 1s core level in H₃BO₃ or
32 B₂O₃ is centered at 193.0 eV (B-O bond), whereas B located in the TiO₂ lattice
33 corresponding to B occupying O sites as B-Ti bond in TiB₂ or O-Ti-B, and interstitial B
34 as Ti-O-B presents lower binding energies at 187.5, 189.6 and 191.7 eV, respectively
35 [16, 18, 19]. The symmetric peak found for all the B-TiO₂ catalysts was at 192.6 eV, thus
36 indicating that B is mainly as H₃BO₃ or B₂O₃ in the catalysts surface, according to XRD
37 results. However, the shift observed from 193.0 eV may be also indicative of the
38 contribution of interstitial B. The presence of substitutional B (O-Ti-B or TiB₂) can be
39 disregarded according to the absence of signal at binding energies lower than 190 eV.
40 Ti 2p spectral region for 12B-TiO₂ and TiO₂ catalysts is depicted in **Fig.2B**. The binding

1 energy of the Ti 2p core levels at 464.5 and 458.7 eV, and the separation of the peaks
2 around 5.8 eV, confirm the valence state of Ti(IV) in TiO₂ [20,21]. However, for 12B-
3 TiO₂ catalysts the peaks have been shifted towards higher binding energy values that
4 can be explained on the basis of the higher electronegativity of boron, thus confirming
5 the formation of Ti-O-B structures (interstitial B) [16]. Finally, **Fig.2C** shows the high-
6 resolution XPS spectra of O 1s spectral region for TiO₂ and 12B-TiO₂ catalysts. The
7 main peak located around 530 eV corresponds to Ti-O bonds with a widening at higher
8 binding energy that has been assigned to hydroxyl groups in the TiO₂ surface. On the
9 other hand, a second contribution to the O 1s spectra is observed in the boron doped
10 catalyst at 532.4 eV corresponding to B-O bonds in H₃BO₃ or B₂O₃ [18]. Boron to
11 titanium atomic surface ratio was calculated for all the catalysts from peak areas and
12 Wagner atomic sensitivity factors [22]. These results are summarized in **Table 1**
13 together with B/Ti bulk ratio calculated from ICP results. It can be noticed that the
14 surface ratios are larger than bulk ratios, suggesting that most of B is located on the
15 surface of TiO₂ during the sol-gel synthesis. This has also been previously reported in
16 La-B co-doped TiO₂ catalysts [14,23].

17 **Table 1** also reports the band gap energy of the catalysts determined according to
18 Tauc's expression from the UV-Vis diffuse reflectance spectra (**Fig.S3** and **Fig.S4** of
19 the supplementary material). The E_g value for bare TiO₂ was 3.07 eV, whereas for B-
20 doped catalysts fluctuated from 3.01 to 3.12 eV with no distinguishable trend with the
21 increasing B content. This is in a good agreement with previous results from Zaleska et
22 al. [18] who reported similar values of E_g for B-doped TiO₂ catalysts with B content from
23 0.5 to 10 wt.%. This is likely the result of low or no mixing of 2p boron bands with 2p
24 oxygen bands since no substitutional B is achieved [5].

25 The catalysts were tested in photocatalysis and photocatalytic ozonation of the
26 selected pesticides DIU, MCPA, TBA and OPP (not shown). However, during the
27 experiments, dissolved boron was detected in the reaction medium, suggesting
28 leaching to some extent. To analyze the leaching phenomenon, the catalysts were
29 submitted to water washing at the same conditions of the reaction medium (catalyst
30 concentration and pH). These results for 12B-TiO₂ photocatalyst are depicted in **Fig.3**
31 together with the evolution of dissolved boron during the photocatalytic ozonation
32 treatment. It can be noticed that unstable boron was leached from the catalyst surface
33 to the aqueous solution just at the beginning of the test and then remained constant up
34 to 2 h. The differences found between pesticides solution or water washing are lower
35 than 1 mgL⁻¹ of B and can be due to experimental deviations.

36 Total boron leached from all the catalysts during the washing procedure is summarized
37 in **Table 2**. Boron concentration in solution reached values as high as 5.5 mgL⁻¹ in the
38 case of the highest loading B-doped catalyst, being the loss of the total boron from 46
39 to 70%. To our knowledge, boron leaching phenomenon has not been previously
40 considered in B-doped TiO₂ catalysts application to wastewater treatment but it is
41 mandatory since the limit of B ions in drinking water is 1 mg L⁻¹ according to the
42 European Union standards [24].

1 On the basis of these results, two of the catalysts were washed with ultrapure water
2 until no dissolved boron was detected (6B-TiO₂-w and 12B-TiO₂-w catalysts). Some
3 characterization results of the washed samples are summarized in **Table 1**. It can be
4 observed a decrease of B bulk content until 0.42-0.49%. The similar percentage of
5 boron after washing both catalysts suggests that only this amount can be introduced in
6 the TiO₂ lattice regardless of the initial amount of boron used. XRD patterns of the
7 washed catalysts do not display the diffraction peak of boron species H₃BO₃ or B₂O₃
8 but, as expected, the washing procedure did not substantially modify the crystal size of
9 the anatase phase. In this line, it is reasonable to assume that no significant changes in
10 the textural properties due to washing procedure develop. On the other hand, the
11 washed catalysts were analyzed by XPS and the results of 12B-TiO₂-w are also plotted
12 in **Fig.2** for comparative purposes. First of all, the intensity of the B 1s core level signal
13 decreased significantly as a result of the loss of boron. However, the peak position
14 located at 191.7 eV confirms the existence of boron in interstitial positions in the TiO₂
15 lattice (Ti-O-B bonds). The Ti 2p and O 1s spectra of 12B-TiO₂-w catalyst were similar
16 to those of bare TiO₂. These results seem to point out that only a small portion of the
17 initial boron was introduced as interstitial boron in the TiO₂ lattice during the sol-gel
18 method used, and also that this B is strongly bonded and stable in aqueous suspension
19 whereas the surface boron forming H₃BO₃ or B₂O₃ entities is easily dissolved. Two
20 extra catalysts were prepared increasing the calcination time from 30 min to 1 h and 3
21 h, but this operating variable did not improve the B stability leading to similar results
22 (not shown). In addition, besides the band gap, other optical properties of the catalysts
23 such absorption and scattering could be modified through B incorporation. The
24 transmitted photon flux through a catalyst suspension could be an indirect
25 measurement of these properties. In that case, the percentage of transmitted photon
26 flux was 58.1% for TiO₂, 47.7% for 6B-TiO₂-w and 76.7% for 12B-TiO₂-w. According to
27 this, 6B-TiO₂-w is expected to make a better use of radiation although no trend with
28 other properties was observed and additional analyses would be necessary to reach
29 stronger conclusions.

30 **3.2. Photocatalytic activity**

31 B-doped washed catalysts were tested in the photocatalytic oxidation and
32 photocatalytic ozonation of the selected pesticides and compared with bare TiO₂ using
33 simulated solar light as radiation source. The evolution of DIU, MCPA, TBA and OPP
34 during photocatalytic oxidation treatment is depicted in **Fig.4**. The catalysts were stirred
35 with the solution of the pesticides in the dark for 30 min to reach the adsorption
36 equilibrium. Low adsorption capacity was observed for DIU, MCPA and OPP whereas
37 around 20% of TBA adsorption was achieved. In general, the adsorption capacity
38 increased in the B-doped catalysts likely due to their more developed surface area and
39 porosity. Direct photolysis of the pesticides did not produce significant degradation of
40 DIU, MCPA and TBA, though a slight decrease of OPP concentration up to 10% was
41 observed. These results are consistent with the UV-Vis absorbance spectra of the
42 target compounds shown in **Fig.S5**. For photocatalytic oxidation with bare and B-doped
43 TiO₂ photocatalysts, in general, the presence of the catalyst improves the depletion

1 rate of all the pesticides, which show different reactivity in the mixture. The order of the
2 reactivity was found to be MCPA>OPP>DIU>TBA. The rate constants of the reaction
3 between these compounds and the hydroxyl radical are $k_{MCPA-HO}=4.5 \times 10^9$, k_{OPP-}
4 $HO=9.8 \times 10^9$, $k_{DIU-HO}=7.1 \times 10^9$, $k_{TBA-HO}=2.8 \times 10^9 \text{ M}^{-1}\text{s}^{-1}$ [25,26]. It is commonly assumed
5 that in photocatalytic oxidation, the main degradation of organics takes place through
6 hydroxyl radicals, especially when direct photolysis and/or adsorption have negligible
7 contributions. The highest degradation rate of MCPA was not in agreement with the
8 order of reactivity derived from the rate constant values. It could be possible that the
9 hydroxyl radical reaction was not the only predominant degradation route for MCPA. In
10 fact, some organic peroxyradicals formed as intermediates during MCPA photocatalytic
11 oxidation are responsible of an autocatalytic behavior, as previously reported [27].

12 The incorporation of B to the catalysts lattice conferred an important effect in its
13 catalytic activity. Thus, the degradation rate of all the pesticides was clearly enhanced
14 in the presence of 6B-TiO₂-w and 12B-TiO₂-w catalysts. Similar behavior was observed
15 for DIU and OPP, as 70-80% degradation was achieved with 12B-TiO₂-w catalyst vs.
16 20-30% obtained with bare TiO₂. For MCPA, around 45 min were necessary to reach
17 almost complete removal whereas around 10% of MCPA still remained in solution with
18 TiO₂ after 120 min of treatment. TBA depletion also improved with B-doped catalysts,
19 reaching around 50% degradation compared to 35% with TiO₂. However, TBA showed
20 a refractory character towards its photocatalytic oxidation, since its concentration
21 decreased faster during the first 15 min and then the degradation rate slowed down.
22 These results point out the benefits of incorporating boron to the TiO₂ lattice. The role
23 of B in interstitial positions of TiO₂ has not been unequivocally defined. It seems that B
24 tends to lose its three valence electrons, which are donated to the 3d states of lattice Ti
25 ions, thus giving rise to Ti(III) species. These latter have been postulated to reduce the
26 recombination of photoexcited electrons and holes [5,28]. A boron content of about 0.5
27 wt.% seems to be enough to enhance the photocatalytic activity of TiO₂. The
28 differences found in the activity of both doped catalysts could be related to the higher
29 content of surface B detected by XPS in the 12B-TiO₂-w catalyst. On the other hand,
30 the differences found in the textural properties and crystallinity of bare TiO₂ and B-TiO₂
31 catalysts might also play an important role in the behavior of the catalysts. However, it
32 has been reported the improvement of photocatalytic performance with the increased
33 crystallinity of the anatase particles since recombination process is prevented to some
34 extent, though larger crystal size leads to lower specific surface areas [29]. Therefore,
35 the improvement observed in the catalytic activity could be related to the presence of
36 boron in TiO₂ interstitial positions more than to the changes produced in TiO₂ crystal
37 size and textural properties. Also, the modification on the radiation absorption and
38 scattering properties cannot be disregarded although transmitted photon flux
39 measurements were not conclusive at this respect.

40 The evolution of the pesticides concentration during photocatalytic ozonation is shown
41 in **Fig.5**. Also, for comparative purposes, ozonation alone and the combination of
42 ozone and radiation (photolytic ozonation) were applied. It can be observed that,
43 regardless of the presence of catalysts and/or radiation, all the ozone treatments led to

1 higher degradation rate of the pesticides than the photocatalytic oxidation process. The
2 average time needed to reach 99% of pesticides removal with ozone treatments was
3 around 60 min for DIU and TBA, and 30 min for MCPA and OPP. These are, in
4 general, in agreement with the values of the rate constants of the ozone-pesticide
5 reaction ($k_{MCPA-O_3}=323$, $k_{OPP-O_3}=379$, $k_{DIU-O_3}=3.7$, $k_{TBA-O_3}=20$ M⁻¹s⁻¹ [25,30,31]).
6 Nevertheless, indirect reactions due to ozone decomposition into hydroxyl radicals
7 could take place at the reaction pH [32,33], also according with the high rate constant
8 values between hydroxyl radical-pesticides commented above.

9 Main differences among the ozone treatments were found in terms of TOC removal.
10 Previously, as seen in **Fig.6**, in all cases, after the dark stage, low TOC removal due to
11 adsorption on the catalysts was observed in comparison of the reaction stage.
12 However, doped catalysts presented higher adsorption capacity compared to bare
13 TiO₂, probably due to their higher surface areas. On the other hand, the TOC removal
14 observed in the direct photolysis run was negligible, as expected. These results were
15 improved by photocatalytic oxidation reaching 25% TOC removal with bare TiO₂ after 2
16 h. This mineralization level increased up to 37% and 45% using 6B-TiO₂-w and 12B-
17 TiO₂-w catalysts, respectively. The higher efficiency of the doped catalysts compared to
18 that of bare TiO₂ was also observed when applying the combined photocatalytic
19 ozonation treatment. Although only 20% of the contaminant mixture was mineralized by
20 single ozonation, the presence of radiation during photolytic ozonation increased up to
21 45% the mineralization degree. In the presence of radiation, a fraction of the ozone
22 molecules that have not directly reacted with contaminants are photolyzed under
23 wavelengths near to 300 nm to produce reactive oxygen species (ROS), which
24 enhance the mineralization rate [34]. These results were highly improved with the
25 photocatalytic ozonation treatment, reaching 65-70% TOC removal. Ozone, as an
26 electrophilic molecule, can trap electrons from the conduction band of the catalyst
27 yielding ozonide ion radicals that decompose into ROS [7,8]. B-doped catalysts were
28 more active than bare TiO₂ and led to faster mineralization rate according to TOC
29 removal reached at 60 min reaction time, though the final mineralization degree was
30 similar (around 1 mg L⁻¹ TOC is the difference between bare and doped-TiO₂ catalysts
31 at the end of the treatment).

32 It is known that hydrogen peroxide can be generated during photocatalytic treatments
33 and also through direct ozone reactions [35,36,37]. The role of H₂O₂ and O₃ involved in
34 photocatalytic reactions has been analyzed through the results depicted in **Fig.7**. When
35 comparing the dissolved ozone profiles (**Fig.7A**) for single ozonation and photolytic
36 ozonation it is observed that ozone accumulated in the solution from the beginning and
37 its concentration remained almost constant along the experiment in contrast to
38 photolytic ozonation which presented a maximum in the ozone concentration, which
39 then decreased dramatically. This suggests that ozone is photolyzed with the radiation
40 used to give rise to ROS, which enhanced the mineralization rate. The low
41 accumulation of ozone in solution during the photocatalytic ozonation experiment can
42 be explained taking into account the electrophilic character of ozone, which can act as
43 an electron acceptor and trap the electrons photogenerated on the photocatalysts

1 surface. On the other hand, the hydrogen peroxide concentration evolution is also
2 shown in **Fig.7B**. Photolysis and photocatalytic oxidation gave place to very low H₂O₂
3 concentrations. However, in all the ozone treatments the concentration of hydrogen
4 peroxide was significantly higher. Thus, the formation of H₂O₂ through direct ozone
5 reactions of the four pesticides was experimentally confirmed. During single ozonation,
6 H₂O₂ concentration increased up to 40 min and then remained almost constant until the
7 end of the experiment. A higher H₂O₂ decomposition rate was observed during
8 photolytic ozonation, resulting in lower concentration at the end of the treatment. The
9 H₂O₂ could undergo photolytic decomposition under wavelengths near 300 nm, thus
10 improving the degradation and mineralization of the contaminants [38]. On the other
11 hand, during photocatalytic ozonation with bare TiO₂ a higher decomposition rate of
12 H₂O₂ was also observed, the concentration being negligible after 100 min of treatment.
13 With B-doped TiO₂ catalysts, the formation of hydrogen peroxide took place at higher
14 rate reaching a maximum concentration at about 20 min and then the consumption was
15 also faster and the concentration negligible at the end of the treatment. These results
16 point out that H₂O₂ is likely being consumed through photocatalytic reactions acting as
17 electron acceptor in the TiO₂ surface. This process is more efficient with B-doped TiO₂
18 catalysts compared to bare TiO₂ also indicating their higher photocatalytic activity.

19 20 **3.3. Catalyst stability**

21 The stability and reusability of the 12B-TiO₂-w catalyst was tested in three consecutive
22 runs of photocatalytic ozonation process. The catalyst was easily separated by
23 sedimentation after each run and used without any treatment in the next experiment.
24 After removing the supernatant solution, a new fresh solution of the four pesticides was
25 added to start the following run. In all the experiments the catalyst from the previous
26 run was kept 30 min in the darkness with the new fresh solution to reach adsorption
27 equilibrium.

28 Taking into account that main differences found between the ozone treatments were
29 found in mineralization, **Fig.8** shows TOC removal percentages during the dark
30 adsorption stage and after 1 and 2 hours of photocatalytic ozonation. During the dark
31 stage, only slight changes were observed in adsorption capacity of the reused catalyst
32 varying the percentage of TOC adsorbed between 3-7% with no trend which indicates
33 that the small amount of initial pesticides adsorbed onto the catalyst surface is oxidized
34 during the photocatalytic treatment. On the other hand, the mineralization reached at 2
35 h reaction time was maintained at about 75% during the consecutive runs.
36 Furthermore, the mineralization rate seems to slightly increase when compared TOC
37 removal at 1 h reaction time being mineralization increased from 55 to 65% during the
38 reutilization of the catalyst. In addition no boron leached was detected after the
39 consecutive use of the catalyst. Therefore, although additional experiments would be
40 needed to test the long term performance of the catalyst, this results point out the
41 stability and reusability of these B-doped TiO₂ catalysts once the non-structural
42 remaining boron was washed.

1 4. Conclusions

2 The sol-gel method used to dope the TiO₂ catalysts led to the incorporation of a lower
3 amount of boron than the theoretical value. A part of the amount of boron on the
4 catalysts was in the form of B₂O₃/H₃BO₃ species, which was unstable in aqueous
5 solution and released boron to the reaction medium. An extra washing of the catalysts
6 with water led to the removal of unstable boron and no further leaching. The rest of the
7 boron on the catalysts was incorporated in interstitial positions of TiO₂ and did not
8 modify the band gap energy with respect to bare TiO₂. The presence of boron on the
9 catalysts also caused the reduction of the crystal size of the anatase particles of TiO₂
10 and an increase of the pore volume and specific surface area respect to the bare TiO₂.
11 The washed B-doped TiO₂ were more active than bare TiO₂ for the removal and
12 mineralization of the target compounds due to the effect of boron in interstitial positions
13 of TiO₂ avoiding the recombination process to some extent. The efficiency of the
14 studied systems regarding mineralization rate followed the order: single ozonation <
15 photocatalysis with TiO₂ < photocatalysis with B-TiO₂ < photolytic ozonation <
16 photocatalytic ozonation with TiO₂ < photocatalytic ozonation with B-TiO₂.
17 Photocatalytic ozonation with B-TiO₂ catalysts was the most efficient process in terms
18 of mineralization, leading to the complete removal of the pesticides in less than 90 min
19 with 75% mineralization after 120 min. The catalytic activity was maintained after 3
20 consecutive runs with no leaching boron detected.

21 Appendix A. Supplementary data

22 Supplementary data associated with this article can be found, in the online version, at
23 XXXXXX

24 Acknowledgements

25 This work has been supported by the Spanish Ministerio de Economía y
26 Competitividad (MINECO) and European Feder Funds through the project CTQ2012-
27 35789-C02-01. Authors acknowledge the SAIUEX service of the University of
28 Extremadura for the characterization analyses. D. H. Quiñones thanks the MINECO the
29 concession of a predoctoral FPI grant and an aid for a research stay at the
30 Loughborough University.

31 References

-
- [1] A. Calzadilla, K. Rehdanz, R. Tol. *J. Hydrology*, 384 (2010) 292-305.
- [2] A. Fujishima, T. N. Rao, D. A. Tryk. *J. Photochem. Photobiol. C Photochem. Rev.* 1 (2000) 1-21.
- [3] X. Gao , P. Chen , J. Liu. *Mater. Let.* 65 (2011) 685–687.
- [4] P. Dharmarajan, A. Sabastiyam, M. Yosuva Suvakin, S. Titus, C. Muthukumar. *Chemical Science Transactions*, 2 (2013) 1450-1458.
- [5] M.V. Dozzi, E. Selli. *J. Photochem. Photobiol. C: Photochem. Rev.* 14 (2013) 13-28.

-
- [6] N. S. Begum, H. M. F. Ahmed, O. M. Hussain. *Bull. Mater. Sci.* 31 (2008) 741–745.
- [7] E. M. Rodríguez, G. Márquez, E. A. León, P. M. Álvarez, A. M. Amat, F. J. Beltrán. *J. Environ. Manag.* 127 (2013) 114-124.
- [8] T.E. Agustina, H.M. Ang, V.K. Vareek, *J. Photochem. Photobiol. C Photochem. Rev.* 6 (2005) 264-273.
- [9] Z. Li, B. Gao, G. Z. Chen, R. Mokaya, S. Sotiropoulos, G. Li Puma. *Appl. Catal. B Environ.* 110 (2011) 50-57.
- [10] V. Loddo, M. Addamo, V. Augugliaro, L. Palmisano, M. Schiavello, E. Garrone. *AIChE J.* 52 (2006) 2565-2574.
- [11] H. Bader, J. Hoigné. *Water Res.* 15 (1981) 449–456.
- [12] W. Masschelein, M. Denis, R. Ledent. Spectrophotometric determination of residual hydrogen peroxide. *Water Management. Water Sewage Works*, August (1977) 69-72.
- [13] F.J. López, E. Giménez, F. Hernández. *Fresenius J. Anal. Chem.* 346 (1993) 984.
- [14] J.W. Liu, R. Han, H.T. Wang, Y. Zhao, W.J. Lu, H.Y. Wu, T.F. Yu, Y.X. Zhang. *J. Mol. Catal. A Chem.* 344 (2011) 145-152.
- [15] S. Bagwasi, B. Tian, J. Zhang, M. Nasir. *Chem. Eng. J.* 217 (2013) 108-118.
- [16] W. Zhang, T. Hu, B. Yang, P. Sun, H. He. *J. Adv. Oxid. Technol.* 16 (2013) 261-267.
- [17] D. Chen, D. Yang, Q. Wang, Z. Jiang, *Ind. Eng. Chem. Res.* 45 (2006) 4110–4116.
- [18] A. Zaleska, J.W. Sobczak, E. Grabowska, J. Hupka. *Appl. Catal. B Environ.* 78 (2008) 92-100.
- [19] E. Finazzi, C. Di Valentin, G. Pacchioni. *J. Phys. Chem. C* 113 (2009) 220-228.
- [20] M.W. Xiao, L. Wang, X.J. Huang, Y.D. Wu, Z. Dang. *J. Alloys Comp.* 470 (2009) 486-491.
- [21] Y. Li, L. Chen, Y. Guo, X. Sun, Y. Wei. *Chem. Eng. J.* 181-182 (2012) 734-739
- [22] C.D. Wagner, L.E. Davis, M.V. Zeller, J.A. Taylor, R.H. Raymond, L.H. Gale. *Surf. Interf. Anal.* 3 (1981) 211-225
- [23] X. Lan, L. Wang, B. Zhang, B. Tian, J. Zhang. *Catal. Today* 224 (2014) 163-170.
- [24] Council of the European Union, Council Directive 98/83/EC of 3 November 1998. On the quality of water intended for human consumption (1998).

-
- [25] M. Olak-Kucharczyk, J.S. Miller, S. Ledakowicz. Ozonation kinetics of o-phenylphenol in aqueous solutions. *Ozone. Sci. Eng.* 34 (2012) 300-305.
- [26] B.A. Wols, C.H.M. Hofman-Caris. *Water Res.* 46 (2012) 2815-2827.
- [27] J. Rivas, R.R. Solis, O. Gimeno, J. Sagasti. *Int. J. Environ. Sci. Technol.* December 2013, DOI 10.1007/s13762-013-0452-4.
- [28] V. Gombac, L. De Rogatis, A. Gasparotto, G. Vicario, T. Montini, D. Barreca, G. Calducci, P. Fornasiero, E. Tondello, M. Graziani. *Chem. Phys.* 339 (2007) 111.
- [29] M.A. Henderson. *Surf. Sci. Reports* 66 (2011) 185-297.
- [30] J.Y. Hu, T. Morita, Y. Magara, T. Aizawa. *Water Res.* 34 (2000) 2215-2222
- [31] F. J. Benítez, F. J. Real, J. L. Acero, C. García. *Water Res.* 41 (2007) 4073 – 4084.
- [32] U. von Gunten. *Water Res.* 37 (2003) 1443-1467.
- [33] F. J. Beltran. *Ozone reaction kinetics for water and wastewater systems.* Boca Raton, CRC Press, 2004, Florida (USA).
- [34] L. Sánchez, X. Domenech, J. Casado, J. Peral. *Chemosphere* 50 (2003) 1085-1093.
- [35] M. Mvula, C. von Sonntag. *Org. Biomol. Chem.* 1 (2003) 1749-1756.
- [36] A. Leitzke, C. von Sonntag. *Ozone Sci. Eng.* 31 (2009) 301-308.
- [37] S. Rakowski, D. Cherneva. *Int. J. Chem. Kinetics* 22 (1990) 321-329.
- [38] J.H. Baxendale, J.A. Wilson. *Trans. Faraday Soc.* 53 (1957) 344-356.

Table 1. Nomenclature and some properties of the B-TiO₂ catalysts

CATALYST	B (wt.%)	d _A (nm)	S _{BET} (m ² g ⁻¹)	V _P (cm ³ g ⁻¹)	(B/Ti) _{ICP} (at./at.)	(B/Ti) _{XPS} (at./at.)	E _g (eV)
TiO ₂	n.d.	16.8	68.3	0.102	0	0	3.07
3B-TiO ₂	0.91	9.9	121.3	0.209	0.068	0.469	3.12
6B-TiO ₂	1.06	9.2	120.1	0.147	0.079	0.531	3.03
9B-TiO ₂	1.81	7.6	122.4	0.163	0.137	0.541	3.05
12B-TiO ₂	3.55	7.5	125.5	0.180	0.273	0.693	3.01
6B-TiO ₂ -w	0.42	9.8	n.m.	n.m.	0.031	0.018	n.m.
12B-TiO ₂ -w	0.49	7.9	n.m.	n.m.	0.036	0.029	n.m.

n.d.: not detected, n.m.: not measured

Table 2. B leaching from the B-TiO₂ catalysts during washing procedure (0.33 g L⁻¹)

CATALYST	B (mg L ⁻¹)	B (%)
TiO ₂	n.d.	n.d.
3B-TiO ₂	1.83	60.6
6B-TiO ₂	1.91	54.3
9B-TiO ₂	4.20	69.9
12B-TiO ₂	5.50	46.6

n.d.: not detected

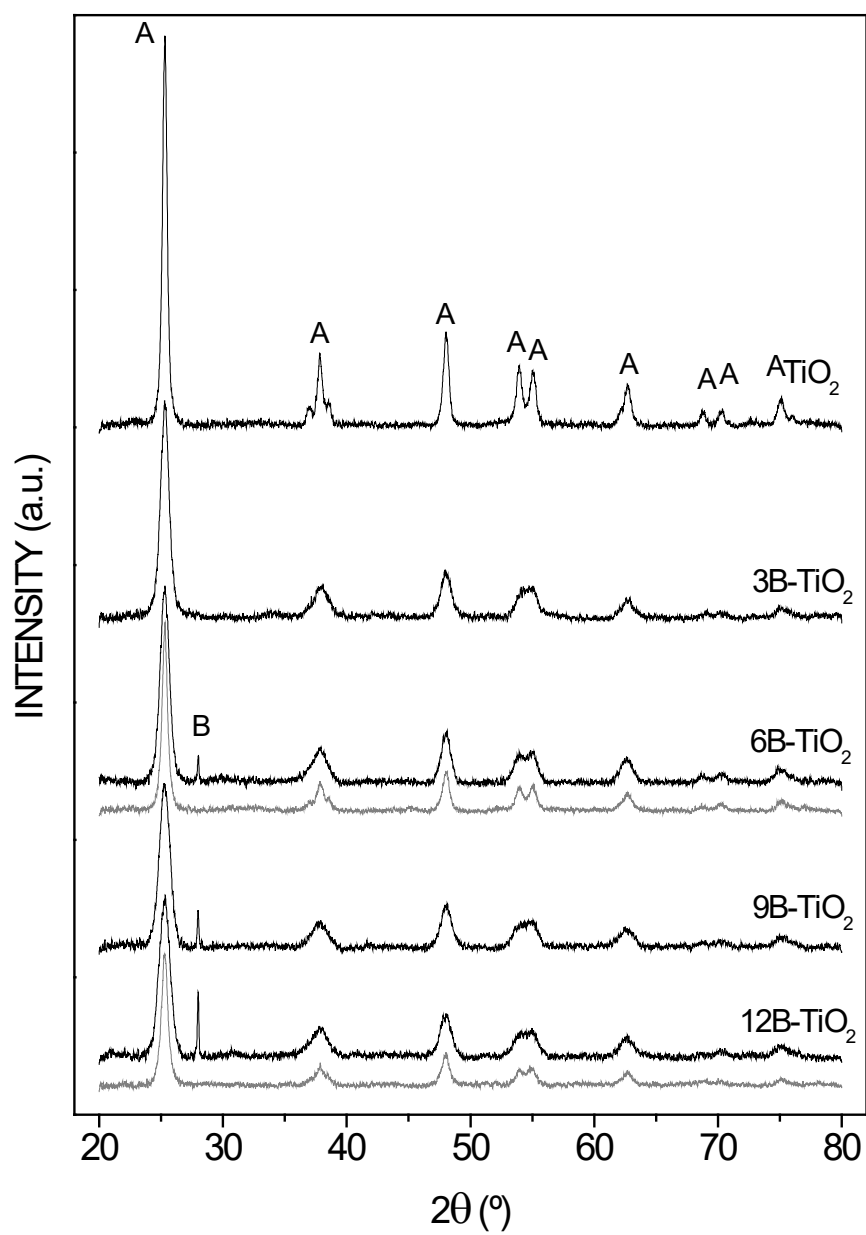


Fig.1. XRD patterns of the photocatalysts (Grey: washed samples, A: anatase, B: boron B₂O₃/H₃BO₃)

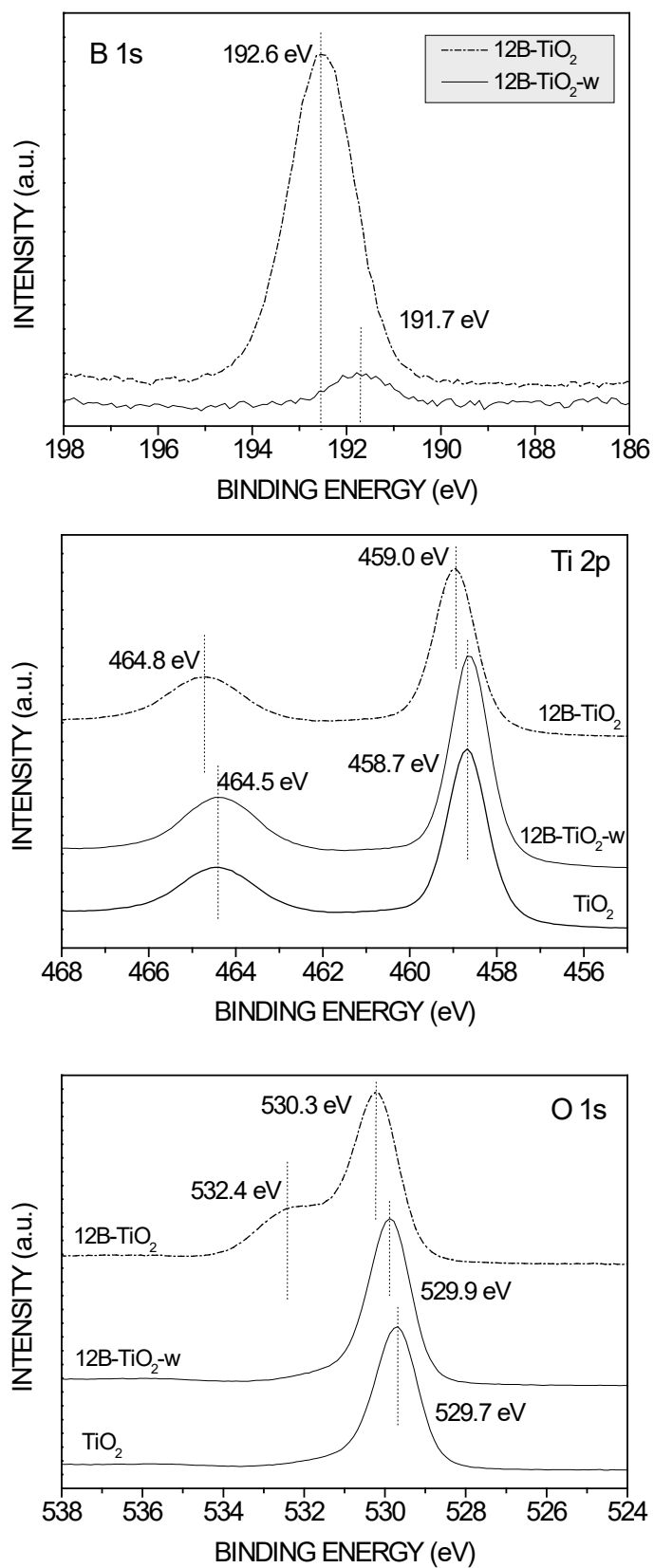


Fig.2. High resolution XPS spectra of B 1s, O 1s and Ti 2p spectral regions of the catalysts TiO₂, 12B-TiO₂ and 12B-TiO₂-w

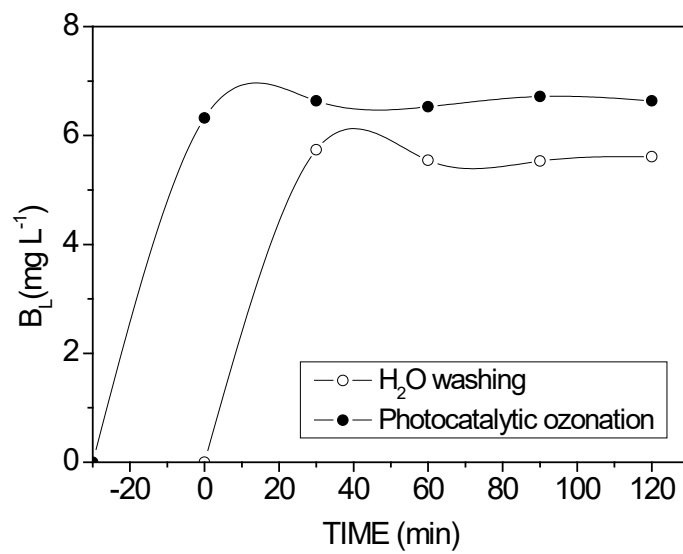


Fig.3. B leaching of the 12B-TiO₂ catalyst during washing procedure and photocatalytic ozonation reaction (0.33 g L^{-1})

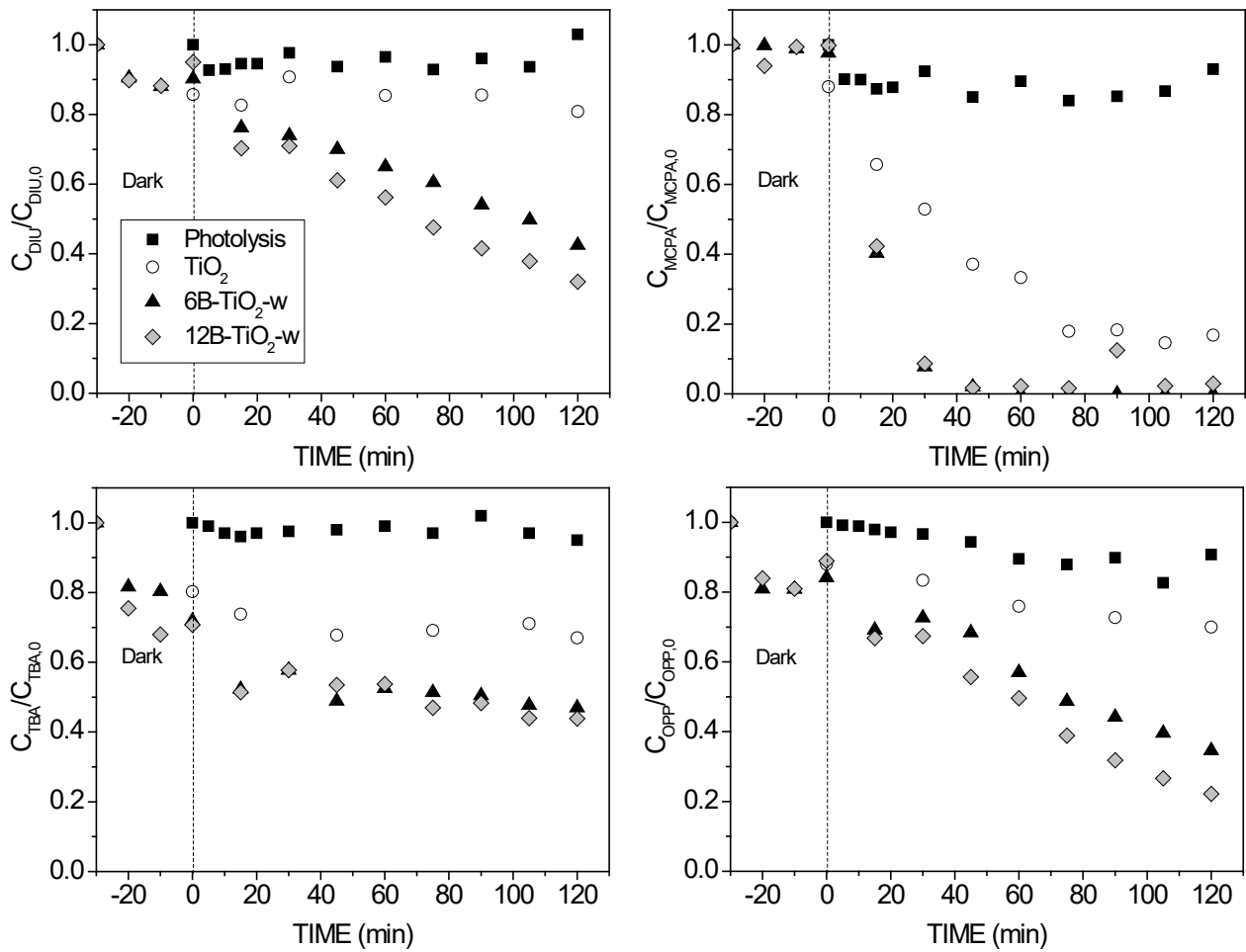


Fig.4. Evolution of dimensionless herbicides and pesticides concentration during photocatalysis with TiO_2 and B- TiO_2 catalysts. Conditions: $pH_0=6.5$, $T=25-40^\circ C$, $C_{PES,0}=5 \text{ mg L}^{-1}$ (in the mixture), $C_{CAT}=0.33 \text{ g L}^{-1}$, $Q_g=10 \text{ L h}^{-1}$ (O_2).

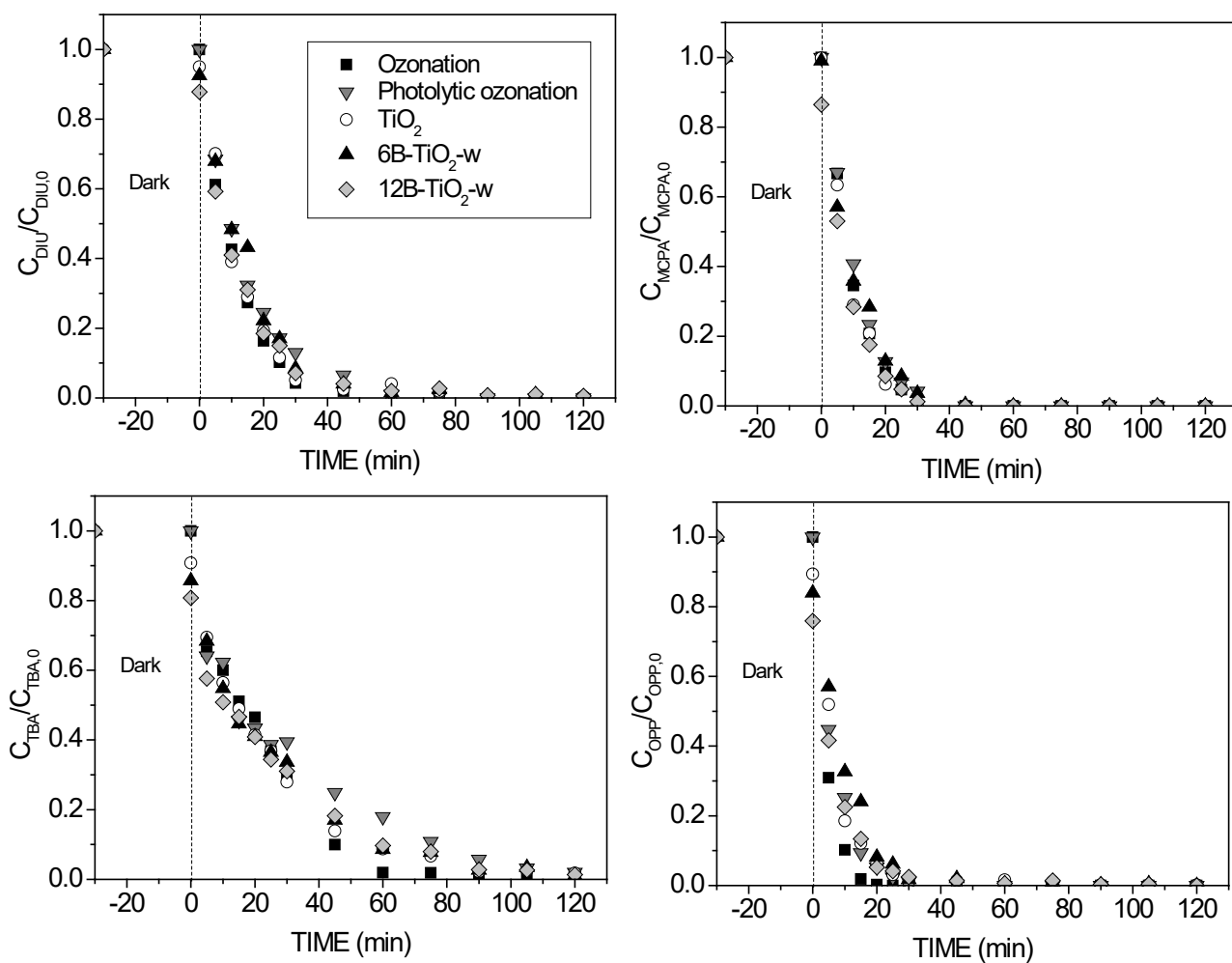


Fig.5. Evolution of dimensionless pesticides concentration during ozone treatments with TiO_2 and B- TiO_2 catalysts. Conditions: $pH_0=6.5$, $T=25-40^\circ C$, $C_{PES,0}=5 \text{ mg L}^{-1}$ (in the mixture), $C_{CAT}=0.33 \text{ g L}^{-1}$, $C_{O_3inlet}=5 \text{ mg L}^{-1}$, $Q_g=10 \text{ L h}^{-1}$ (O_3/O_2).

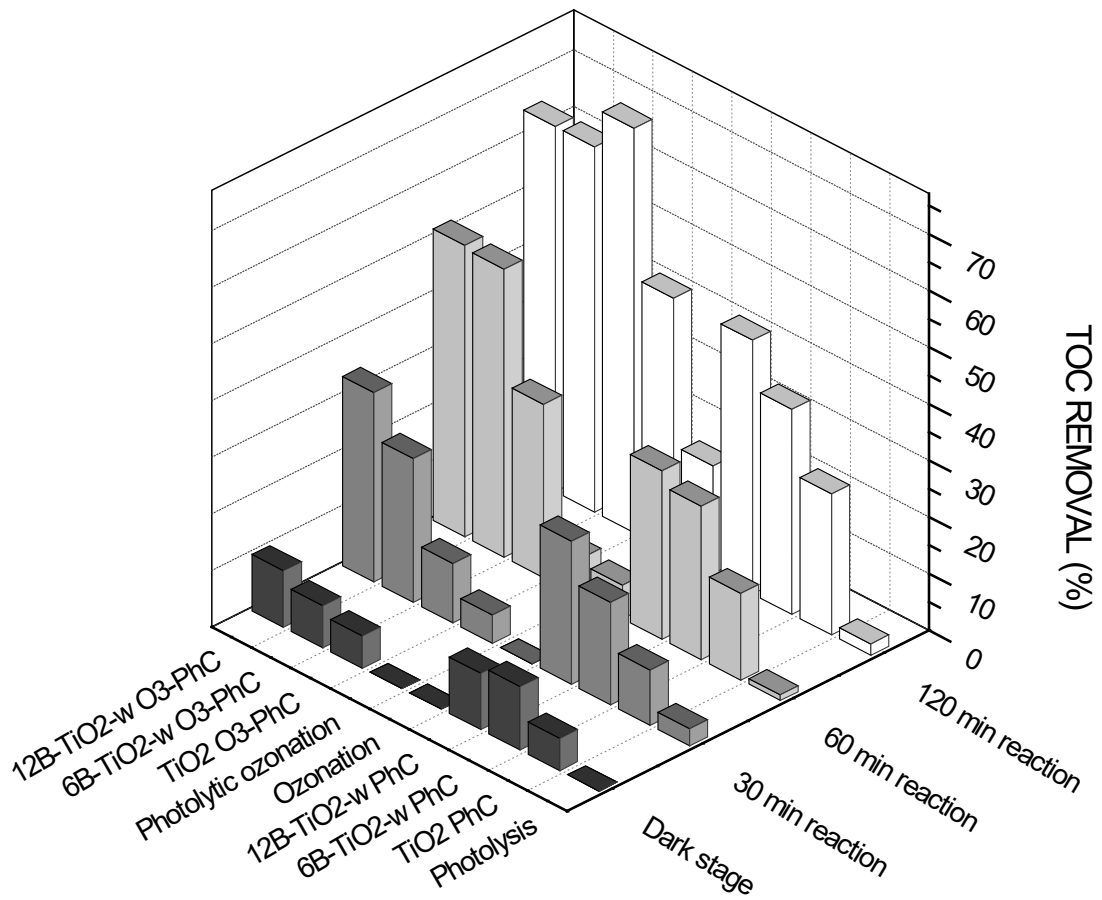


Fig.6. TOC removal during all the treatments applied with TiO₂ and B-TiO₂ catalysts. Conditions: pH₀=6.5, T=25-40°C, C_{PES,0}=5 mg L⁻¹ (in the mixture), C_{CAT}=0.33 g L⁻¹, C_{O₃inlet}=5 mg L⁻¹, Q_g=10 L h⁻¹ (O₃/O₂).

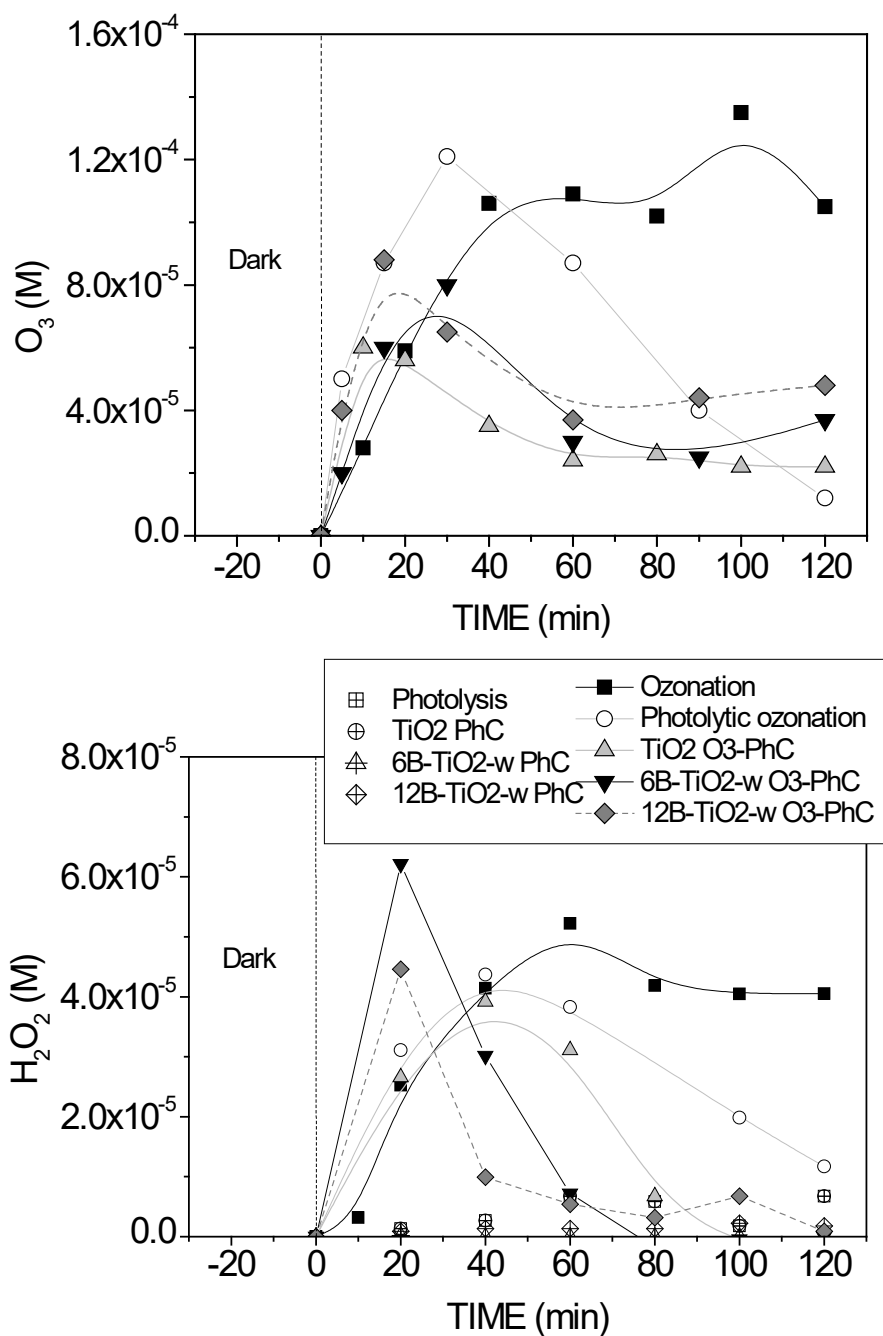


Fig.7. Evolution of dissolved O_2 and H_2O_2 concentrations during all the treatments applied. Conditions: $pH_0=6.5$, $T=25-40^\circ C$, $C_{PES,0}=5 \text{ mg L}^{-1}$, $C_{CAT}=0.33 \text{ g L}^{-1}$, $C_{O_3 \text{ inlet}}=5 \text{ mg L}^{-1}$ (in the mixture), $Q_g=10 \text{ L h}^{-1}$ (O_3/O_2).

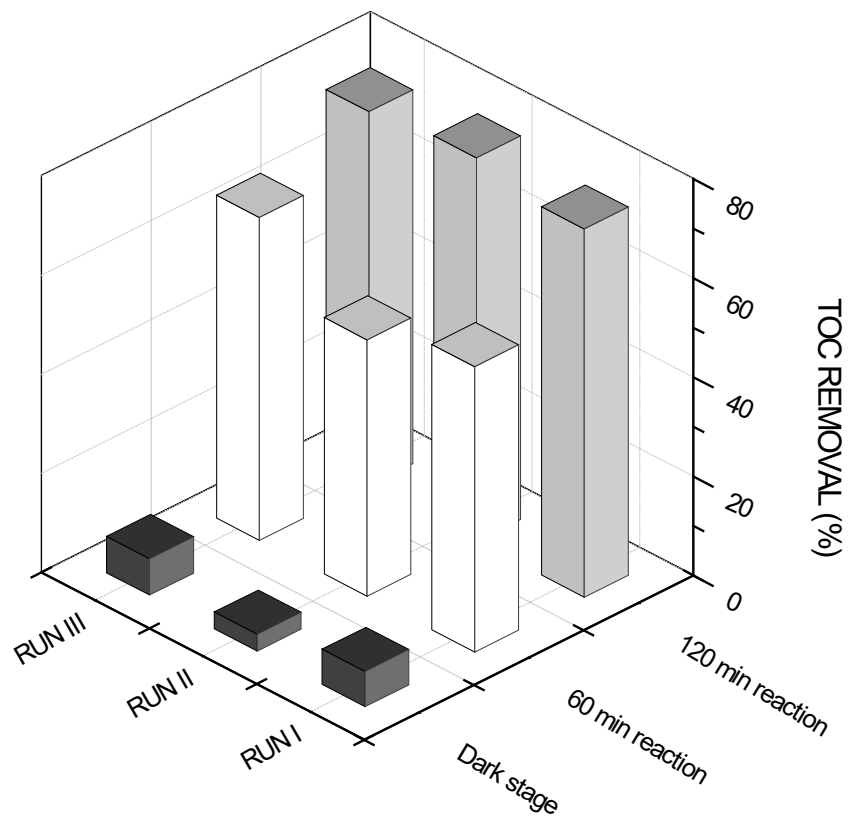


Fig.8. TOC removal during consecutive photocatalytic ozonation runs. Conditions: $pH_0=6.5$, $T=25-40^\circ\text{C}$, $C_{PES,0}=5 \text{ mg L}^{-1}$ (in the mixture), $C_{CAT}=0.33 \text{ g L}^{-1}$, $C_{O_3\text{ginlet}}=5 \text{ mg L}^{-1}$, $Q_g=10 \text{ L h}^{-1}$ (O_3/O_2).